Precursors to stress-induced martensitic transformations and associated superelasticity: Molecular dynamics simulations and an analytical theory

Xiangdong Ding,[1,2] Tetsuro Suzuki,[1,3] Xiaobing Ren,[1,2,3,*] Jun Sun,[1,2] and Kazuhiro Otsuka[1,3]
[1]*Multidisciplinary Materials Research Center, Xi'an Jiaotong University, 710049, Xi'an, People's Republic of China*
[2]*State Key Laboratory for Mechanical Behavior of Materials, Xi'an Jiaotong University, 710049, Xi'an, People's Republic of China*
[3]*Ferroic Physics Group, National Institute for Materials Science, Tsukuba 305-0047, Japan*
(Received 22 May 2006; revised manuscript received 8 August 2006; published 20 September 2006)

Precursor phenomena are critical issues for martensitic transformation, as they provide important clues for understanding the origin of the transformation and the structure of the transformation products. Prior to temperature-induced martensitic transformation, it has been recognized for a long time that the basal plane shear modulus C' ($\{110\}\langle 1\bar{1}0\rangle$ shear mode) of the parent phase decreases on approaching the transformation temperature. On the other hand, martensitic transformation can also be induced by stress; but little has been known about whether similar precursor phenomenon also exists prior to such stress-induced martensitic transformation. In the present study, we successfully simulated the stress-induced martensitic transformation and associated superelasticity in a generic martensitic system by means of molecular dynamics method. Through calculating C' as a function of applied stress, we found a significant softening of C' prior to the stress-induced martensitic transformation. This is a clear evidence for the existence of lattice softening prior to stress-induced martensitic transformation. Our results suggest that lattice softening is a common feature for both temperature- and stress-induced martensitic transformation. An interesting result is that stress does not soften all the crystallographically equivalent $\{110\}\langle 1\bar{1}0\rangle$ shear moduli (all are C' by definition); it softens some of them while it hardens the rest. This is contrasting with the temperature-induced C' softening, in which all equivalent $\{110\}\langle 1\bar{1}0\rangle$ shear moduli simultaneously soften to the same extent. It corresponds to the well-observed fact for given stress direction only certain martensite variant(s) are induced while other variants are prohibited. We also formulated an analytical theory to investigate the variation of C' under stress, and obtained similar result as that of our molecular dynamics simulations.

DOI: 10.1103/PhysRevB.74.104111 PACS number(s): 64.70.Kb, 63.70.+h, 64.60.−i, 71.15.Pd

I. INTRODUCTION

Martensitic transformation (MT) is a displacive, diffusionless first-order transformation from a high-symmetry phase at high temperature to a low-symmetry phase (martensite) at low temperature. It has been extensively studied for decades because of its importance in metallurgy and its key role in shape memory phenomenon.

An interesting feature of martensitic transformation in shape memory alloys is the existence of precursor phenomena,[1,2] which announce the instability of the system towards a martensitic phase. Prior to temperature-induced martensitic transformation, many important precursor phenomena in various shape memory alloys have been observed by various methods. Elastic constant measurements[3–9] always show a softening of elastic constant C' [$\equiv(C_{11}-C_{12})/2$, which reflects the resistance to $\{110\}\langle 1\bar{1}0\rangle$ shear] prior to martensitic transformations; Neutron scattering experiment in most cases[10–13] confirms a low-lying TA2 acoustic phonon which further softens with approaching transformation temperature. Elastic neutron scattering in most cases reveals a central peak,[13] and x-ray diffraction reveals diffuse scattering and extra diffuse spots,[14] These suggest the existence of static martensitelike structure above the transformation temperature. Many TEM observations reported diffuse streaks along $\langle 110\rangle$ directions and in some cases discrete diffuse spots were observed.[15,16]

Among these phenomena, the anomalous dynamical response of the lattice to some specific displacements are intimately related to the transformation mechanism and have been reported to occur in all bcc martensitic system investigated so far, i.e., all bcc martensitic materials exhibit a low-lying TA2 (110) $\langle 1\bar{1}0\rangle$ phonon branch, which corresponds to a low value of the elastic constant C'. Both the elastic constant and the TA2 phonon soften on approaching the transformation temperature.

On the other hand, stress can also induce martensitic transformation. However, little is known about whether the above-mentioned precursor phenomena exist prior to stress-induced MT. This is mainly due to the difficulty in experimentation under stress. The change of phonon energy and elastic constant with stress reflects the anharmonicity of the lattice. Previous investigations about the third order elastic constants[2,5,17–20] and Gruneisen parameters[2,20–22] indicate enhanced anharmonicity close to the transition temperature, but these studies measured anharmonicity effect only for low stress level. It is not clear how the lattice dynamic properties change from zero stress up to the critical stress at which martensite is induced. The investigation of this important problem may provide new insights into the underlying mechanism of martensitic transformation under stress.

The purpose of the present work is to use molecular dynamics (MD) simulations approach to explore this important issue. So far, most MD simulations of martensitic transformations have focused solely on temperature-induced MT,[23–27] and no simulations for stress-induced MT and its related precursor effect have been done to date. This is mainly due to the lack of appropriate potential function.

In the present study, we applied an appropriate Lennard-Jones potential function and successfully simulated the stress-induced martensitic transformation of a generic martensitic system. Our simulations reproduced the characteristic superelastic deformation behavior associated with the stress-induced transformation. This indicates that our simulations capture the essential physics of the martensitic system. Then we focus on the possible softening of elastic constant C' prior to stress-induced MT by MD simulations. Our result clearly shows significant softening in C' prior to the stress-induced MT, proving the existence of lattice softening before stress-induced MT. Furthermore, our simulations provide the microscopic information in atomic level about C' softening prior to stress-induced MT, and point out the difference in C' softening between temperature-induced and stress-induced MT.

The layout of this paper is as follows: first, in Sec. II, we introduce the analytical formula of elastic constants C' under stress, which is the basis for calculating the change of C' with stress prior to stress-induced MT. Section III focuses on the molecular dynamics simulations. Then in Sec. IV, we compare our results with thermodynamic theory, and prove elastic softening prior to stress-induced MT by an analytical theory, and then make a comparison between temperature- and stress-induced MT. Finally, the conclusions are made in Sec. V.

II. BASIC FORMULA OF ELASTIC CONSTANT C' UNDER FINITE STRESS

The physical meaning of C' is the "stiffness" against a $\{110\}\langle 1\bar{1}0\rangle$ type shear ($\{110\}$ shear along $\langle 1\bar{1}0\rangle$ direction). Accordingly, C' under a finite shear stress τ_j exerted on the system (as in our case) can be calculated as follows:

$$C_i'(\tau_j) \equiv \left.\frac{d\tau_i}{d\gamma_i}\right|_{\tau_j}, \tag{1}$$

where τ_j is the finite shear stress and $d\tau_i$ and $d\gamma_i$ are the infinitesimal shear stress and strain, respectively. The subscript i and j denote a particular $\{110\}\langle 1\bar{1}0\rangle$ type shear mode of the infinitesimal shear stress $d\tau_i$ and that of the finite shear stress τ_j; it can be (110) $[1\bar{1}0]$, (101) $[\bar{1}01]$, or (011) $[0\bar{1}1]$ shear mode.

When there is no finite stress exerted on the system, the elastic moduli C_i' for different $\{110\}\langle 1\bar{1}0\rangle$ type shear modes are the same, as different $\{110\}\langle 1\bar{1}0\rangle$ type shear modes in a cubic system are equivalent. However, under finite stress, the crystal is slightly distorted and has a lower symmetry; as the result, the C_i' may take different values for different $\{110\}\langle 1\bar{1}0\rangle$ type shear mode i under the finite stress τ_j.

Equation (1) shows that to obtain C' under finite shear stress τ_j, we should first apply the finite shear stress τ_j, followed by superimposing on it a small shear stress $d\tau_i$ and then measuring its resultant small shear strain $d\gamma_i$. However, our MD software has difficulty to generate a shear stress, although it can produce tensile and compressive stresses.

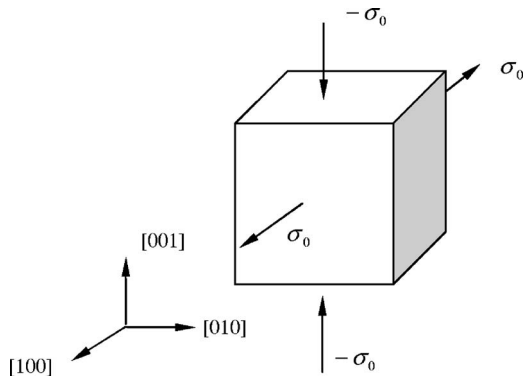

FIG. 1. Sketches of the geometrical configuration of biaxial stress case relative to the crystal. Symbols used here: σ_0, external stress.

Thus we cannot directly use Eq. (1) to calculate the elastic constant C' of a $\{110\}\langle 1\bar{1}0\rangle$ shear mode under stress. This difficulty can be circumvented by noticing the equivalence of a pure shear stress state with a tension-compression biaxial stress state. For example, the stress state of a pure (101) $[\bar{1}01]$ shear mode is equivalent to a tension-compression biaxial stresses σ_0 along [100] and $-\sigma_0$ along [001] direction, as shown in Fig. 1. Considering such an equivalence, C' can be expressed in terms of the biaxial stress and strain

$$C_i'(\sigma_j) = \left.\frac{d\sigma_i}{d\varepsilon_i}\right|_{\sigma_j}, \tag{2}$$

where σ_j is the biaxial stress equivalent to finite $\{110\}\langle 1\bar{1}0\rangle$ shear stress τ_j, $d\sigma_i$, and $d\varepsilon_i$ are the infinitesimal biaxial stress and strain corresponding to $d\tau_i$ and $d\gamma_i$, respectively.

Equation (2) provides an explicit and simple method for the measurement of elastic constant C' as a function of finite shear stress for different $\{110\}\langle 1\bar{1}0\rangle$ modes. Our MD simulations uses this method to calculate the variation of $C_i'(\sigma_j)$ with biaxial stress σ_j. The finite biaxial stress σ_j is first exerted on the crystal (represented by a "super cell" that comprises thousands of unit cells of the crystal), and the dimension change of the super cell is monitored. Then a small "measuring stress" $d\sigma_i$ is applied on the strained super cell along an appropriate $\{110\}\langle 1\bar{1}0\rangle$ orientation, followed by measuring the resultant small strain change $d\varepsilon_i$, which is obtained by measuring the distortion of the super cell by this "measuring stress" relative to the cell shape under finite stress σ_j only. The elastic constant C' along this particular orientation is then calculated by Eq. (2).

III. MOLECULAR DYNAMIC SIMULATION

A. Computational modeling

MD simulations were carried out with a commercial software "Materials Explorer 2.0," which is based on the Parrinello-Rahman method.[28] In this method, the external stress is directly introduced to the Lagrangian equations of motion. To begin with the MD simulations, an external stress

TABLE I. Parameters in Eq. (3).

$r_{11}(10^{-10}$ M)	$r_{22}(10^{-10}$ M)	$r_{12}(10^{-10}$ M)	$e_{11}(10^{-27}$ J)	$e_{22}(10^{-27}$ J)	$e_{12}(10^{-27}$ J)
1.0000	0.8494	0.8947	1.133 75	1.033 87	1.249 00

is exerted on the system, and a long run is needed to establish the equilibrium of the system under the external stress; then the corresponding strain can be obtained by calculating the variation of the Parrinello-Rahman cell (super cell) axis lengths. By repeating the above steps, the corresponding strain at different external stress can be obtained. Of course, the external stress should be zero in the first run to establish the reference equilibrium state of the system.

Unfortunately, due to the lack of a proper potential energy function, this software could not simulate martensitic transformation. In this work, a special 8-4 Lennard-Jones potential (instead of the standard 12-6 Lennard-Jones potential) was introduced into the software to simulate the martensitic transformation. This 8-4 potential was proposed originally by Sanchez *et al.*,[29] to study the phase diagrams of Ni-Al alloy and later extended to a wide range of binary alloys by Shimono and Onodera.[30] Recently Suzuki and Shimono[24] showed that this potential is capable of simulating the temperature-induced MT.

By using this potential, we are able to simulate the martensitic transformation of a "generic" martensitic system that undergoes a $B2$ to $L1_0''$ (an $L1_0$ based orthorhombic structure) transformation.[23,24] As will be seen later, our simulations of this generic martensitic system capture the essential physics of martensitic transformation and the effect of external stress.

The expression for two-body 8-4 potential V_{ab} can be written as follows:

$$V_{ab}(r) = e_{ab}\{(r_{ab}/r)^8 - 2(r_{ab}/r)^4\}, \tag{3}$$

where e_{ab} and r_{ab} represent the bond strength between atoms and the atomic size respectively. For our model $B2$ crystal, these two parameters are chosen from that of a typical martensitic system Ti-Ni, the values of e_{ab} and r_{ab} are shown in Table I. The mole mass of the atoms in our model $B2$ crystal are set to be 47.9 g/mol (Ti atom) and 58.7 g/mol (Ni atom) respectively, the density of Ti atom and Ni atom are 4.5 g cm^{-3} and 8.9 g cm^{-3}, respectively. But one should not expect that such a simple potential can generate the complex B19′ martensite of Ti-Ni; the martensite with the above potential should be considered.

Furthermore, the isothermal-isobaric ensemble was adopted, and the initial MD cell (with $B2$ structure) was built up in a cubic box containing 3456 atoms (1728 Ti atoms and 1728 Ni atoms). To avoid the existence of the free surface in the MD cell, periodic boundary conditions were imposed in three dimensions.

B. Temperature induced martensitic transformation

As the stress-induced MT occurs in the parent state, i.e., at a temperature above the transformation temperature, we need to know first the transformation temperatures. They are M_s (martensite-start temperature upon cooling), M_f (martensite-finish temperature upon cooling), A_s (reverse-transformation-start temperature upon heating), and A_f (reverse-transformation-finish temperature upon heating). For this purpose, we first simulated martensitic transformation during temperature cycles to determine these temperatures of our ensemble.

The simulation started with an ensemble of parent phase ($B2$ structure) at 300 K. After 20 picoseconds (ps) thermal holding, cooling procedure started and the ensemble was cooled from 300 K to 0.1 K in 60 ps. In the subsequent 40 ps, the temperature of the system was kept at 0.1 K to get the equilibration of the low temperature phase. Then the ensemble was heated up to 300 K again in 60 ps. The variation of temperature with time is shown in Fig. 2.

The Parrinello-Rahman cell axis lengths, which are related to the size and shape of the unit cell of our model crystal, are shown as a function of time in Fig. 2. It is found that the length of three cell axes keep almost the same until the temperature (T) reaches 196 K, which means that $B2$ structure (parent phase) is stable down to 196 K. When the system is cooled from 196 K to 189 K, the cell lengths change abruptly; indicating that the $B2$ structure immediately transforms into a close-packed structure labeled $L1_0''$. When the system is heated up to 249 K again, the values of lattice constants again changed suddenly, and this sudden change finishes at 254 K. On further heating, the value of lattice constants remained stable and expanded continuously.

As shown in Fig. 2, by introducing a proper potential function, we can successfully simulate temperature-induced MT. Furthermore, the average M_s temperature for four runs of the $B2$ to $L1_0''$ transformation turns out to be 196 K, and the corresponding A_s temperature is 249 K, while the aver-

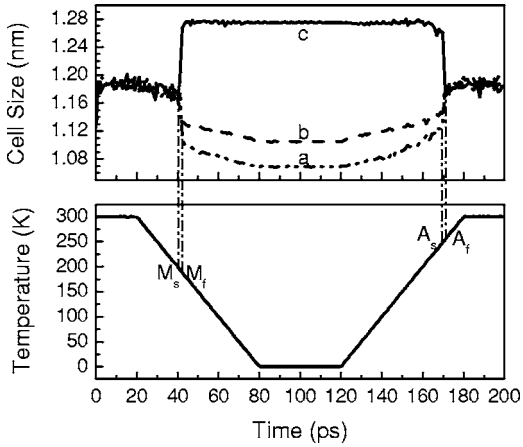

FIG. 2. The Parrinello-Rahman cell axis lengths and temperature are shown as a function of time. The cell is related to the size and shape of the unit cell of a completely ordered $B2$ crystal with 3456 atoms.

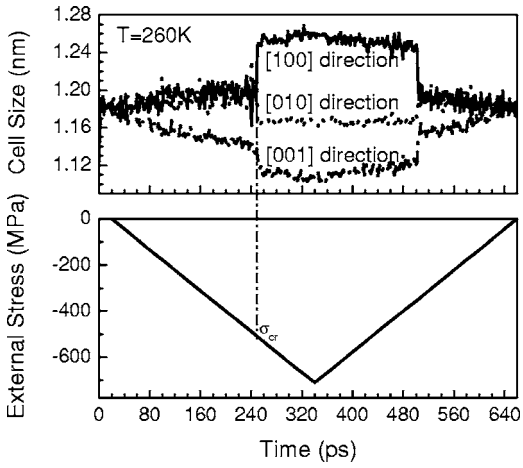

FIG. 3. The Parrinello-Rahman cell axis lengths and uniaxial compressive stress along [001] direction are shown as a function of time. The cell is related to the size and shape of the unit cell of a completely ordered $B2$ crystal with 3456 atoms. Symbols used here: σ_{cr}, Stress-induced martensitic transformation starting stress.

age M_f temperature is 189 K, and the average A_f temperature is 254 K. The hysteresis of the present phase transformation is about 59 K, which indicates the present MT is a first order phase transformation.

C. Uniaxial and biaxial stress induced martensitic transformation

With the information of transformation temperatures of the ensemble, we can now simulate stress-induced MT. Initially, the temperatures of the ensemble were cooled from 300 K to a given temperature in 20 ps, which is higher than M_s (196 K), and were held for 20 ps to establish equilibrium, and then an external stress was applied.

As we know, when a martensitic system is stressed above the A_f point, superelasticity occurs, while a martenstic system is stressed among M_s and A_f point, we can only get partial superelasticity. Now we show the results of our MD simulations.

First, a uniaxial compressive stress was applied along [001] direction at 260 K to simulate the superelastic behavior; the loading rate was 20 N/ps. The variations of cell size and external stress with time were shown in Fig. 3. To facilitate the description below, the martensitic-transformation-start stress upon loading is defined as the critical stress (σ_{cr}), which was shown in Fig. 3.

When a uniaxial compressive stress is applied along [001] direction of the ensemble, there is a contraction in the [001] direction and an expansion in [010] and [100] direction. This elastic deformation behavior continues until the applied stress reaches a critical stress, which is 510 MPa at 260 K. However, as shown in Fig. 3, the fluctuation of lattice constants prior to stress-induced MT are much higher than those of temperature-induced MT shown in Fig. 2, so it is difficult to obtain the corresponding compressive strain directly.

In the present MD simulation, a long run of 2000 time steps was carried out for a given loading. All the compressive strain corresponding to the applied stress was calculated with the last 1000 time steps of this run, and a method of 10 data-point smoothing was used to smooth compressive strain versus time curves.

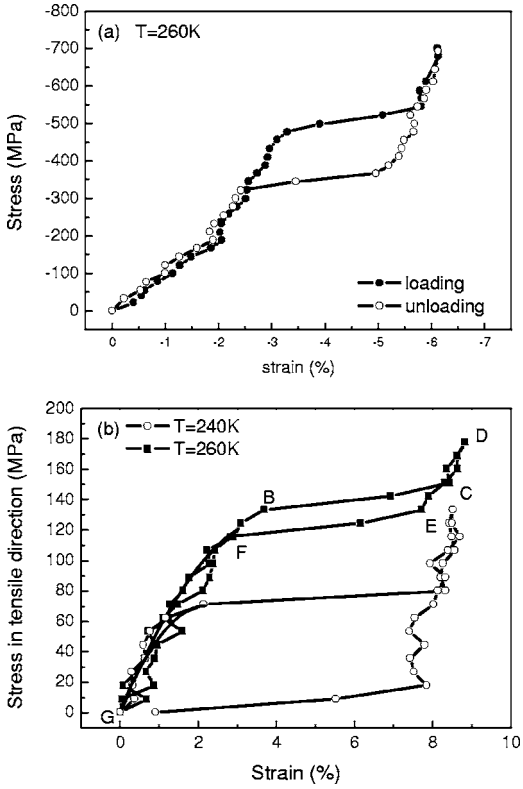

FIG. 4. Simulated stress-strain curves of our $B2$ model crystal (a) at 260 K for the case of uniaxial compression. The curve was calculated from Fig. 3; (b) at different temperature for the case of biaxial stress state shown in Fig. 1.

The calculated compressive stress-strain curve along [001] direction at 260 K is shown in Fig. 4(a). It is clear that the superelasticity, which is caused by the stress-induced transformation and the reverse transformation on unloading, has been simulated successfully. It shows that the introduced potential function can successfully describe both temperature- and stress-induced MT.

Then, MD simulations for biaxial stress state shown in Fig. 1, was done to calculate the variation of elastic constant C' prior to stress-induced MT according to Eq. (2). In the present calculation, an external tensile stress is applied along [100] direction, and a compressive stress is simultaneously applied along [001] direction. The loading rate along [100] and [001] direction are 10 N/ps.

Figure 4(b) shows the simulated stress-strain curves along [100] directions for [100]-[001] biaxial stress state. When the temperature of the ensemble is 260 K, which is higher than A_f (254 K), we can see that the stress-strain behavior in biaxial loading is very similar to the case of uniaxial loading shown in Fig. 4(a). On loading, the system deforms elastically until point B is reached, from which $L1_0''$ martensitic transformation starts to form. As the loading increases, the deformation proceeds by the stress-induced MT from point B to point C on the stress-strain curve and form a plateau. The

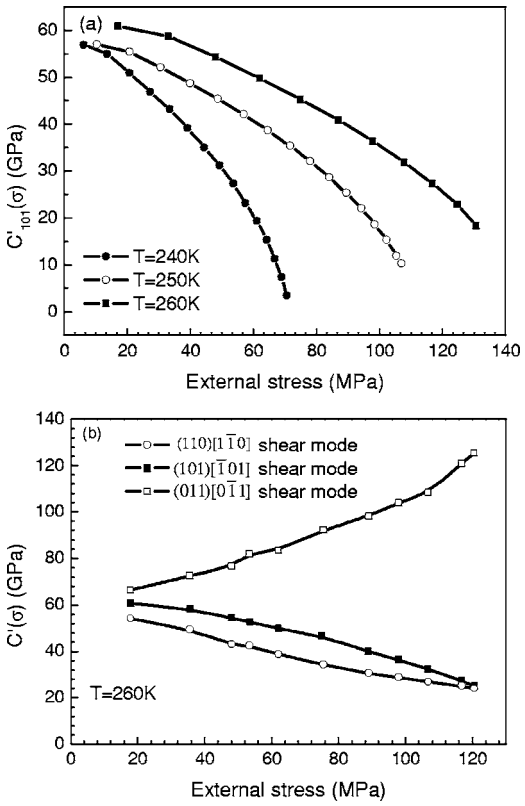

FIG. 5. Predicted elastic constant $C'(\sigma)$ by MD simulations (a) of $(101)[\bar{1}01]$ shear mode as a function of the applied stress prior to the $B2$-$L1_0''$ transformation at different temperature; (b) of three crystallographially equivalent shear modes prior to the stress induced $B2$-$L1_0''$ transformation at constant temperature. The biaxial stress is applied alone [100]-[001] orientation as shown in Fig. 1. Symbols used here: $C'_{101}(\sigma)$, $C'(\sigma)$ of $(101)[\bar{1}01]$ shear mode.

applied stress at point B is defined as the critical stress. From point C to point D, it deforms elastically again. On unloading, the strain recovers elastically from point D to near point E first, and then it recovers more quickly by the reverse transformation from the $L1_0''$ to $B2$ structure (point E-F). When the loading is completely removed, the ensemble recovers to its original structure (point G).

When the temperature of the ensemble is 240 K, which is among M_s and A_f, we can only get a partial superelasticity [shown in Fig. 4(b)], which is also consistent with the well-known experimental observation. It is clear from these observations that superelastic behavior can also be induced in biaxial stress mode or an equivalent pure shear mode.

Based on the above, we can calculate the elastic constant $C'(\sigma)$ of different shear mode at the given [100]-[001] biaxial stress mode shown in Fig. 1. First, we keep the [100]-[001] biaxial stress σ_0 as constant, then apply an infinitesimal tension-compression stress along [100]-[001] direction, [100]-[010] direction, and [010]-[001] direction, respectively. According to Eq. (2), $C'(\sigma)$ of three crystalgraphically equivalent shear mode at the given stress σ_0 can be obtained.

Figure 5(a) shows the relationship between $C'_{101}(\sigma)$ [i.e., $C'(\sigma)$ of $(101)[\bar{1}01]$ shear mode] and external stress at different temperature for the present biaxial state. First, we can see that the elastic constant $C'_{101}(\sigma)$ shows a significant softening with the increase of the applied stress at constant temperature. It is further noted that the softening is not linear with respect to stress. All of above are very similar to those of temperature-induced MT. This indicates that elastic constant softening is a common feature both in temperature- and stress-induced MT. Furthermore, $C'_{101}(\sigma)$ decreases with the decrease of temperature at given applied stress, which is similar to the elastic softening prior to temperature-induced MT without external stress. It also proves the validity of the present calculation.

Figure 5(b) shows the relationship between $C'(\sigma)$ of different crystallographically equivalent shear modes and external stress at a constant temperature (260 K). We can see that, at a given temperature (260 K), $C'(\sigma)$ softens only in $(110)[1\bar{1}0]$ and $(101)[\bar{1}01]$ shear modes and hardens in $(011)[0\bar{1}1]$ shear mode for the present biaxial stress state, which is different from that of temperature-induced MT. We will discuss it in the following sections.

D. Atomic configurations prior to stress-induced martensitic transformation

From the above results, we can confirm that elastic constant C' in some specific directions soften with the increase of applied stress prior to stress induced MT. However, what is the corresponding microscopic picture at atomic levele? To find the answer, we show the variation of atomic configurations prior to stress-induced MT.

In our MD simulations, the ideal crystal structure of parent phase is $B2$ phase [shown in Fig. 6(a)], while that of martensitic phase is $L1_0''$ phase, as shown in Fig. 6(b). For the case of biaxial stress state shown in Fig. 1, Fig. 6(c)–6(e) show the variation of atomic configurations viewed in different directions when the applied stress increases from zero to critical stress. Viewed from $[001]_{B2}$ direction [Fig. 6(c)], we can see that, four clusters which move along $(110)[1\bar{1}0]$ direction are formed prior to critical stress, and the atoms in the adjacent two clusters move along (100)[100] direction. If viewing from $[010]_{B2}$ direction [Fig. 6(d)], we can also find four clusters, which move along $(101)[\bar{1}01]$ directions, are also formed prior to critical stress. However, if viewed from $[100]_{B2}$ direction [Fig. 6(e)], we cannot see there exists obvious clusters prior to critical stress. These indicate that, clusters are formed only in $(110)[1\bar{1}0]$ and $(101)[\bar{1}01]$ shear mode, but not in the crystallographically equivalent $(011)[0\bar{1}1]$ shear mode for the present biaxial stress condition. As will be seen later, such nonequivalence in clustering is related to the nonequivalence in the C' softening along different $\{110\}\langle 1\bar{1}0\rangle$ shear mode, and also related to the selected formation of martensite variants by stress.

IV. DISCUSSION

A. Comparison between simulated result and thermodynamic theory

To verify the present MD simulations, we first compared the simulated results with thermodynamic theory.

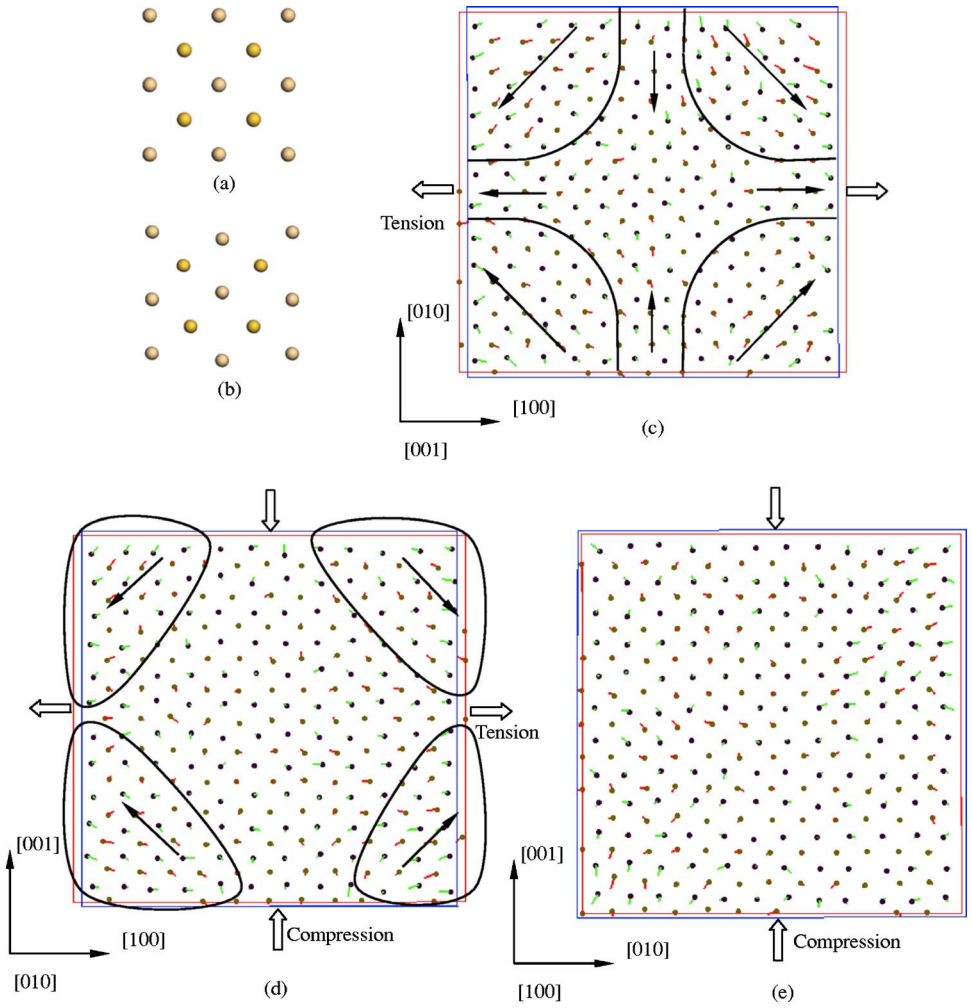

FIG. 6. (Color online) Atomic configuration during temperature induced and stress induced martensitic transformation. (a) ideal $B2$ structure; (b) ideal martensitic structure; (c) variation of atomic configurations between 0 and σ_{cr} viewed from $[001]_{B2}$ direction for the case of biaxial stress state; (d) variation of atomic configurations between 0 and σ_{cr} viewed from $[010]_{B2}$ direction for the case of biaxial stress state; (e) variation of atomic configurations between 0 and σ_{cr} viewed from $[100]_{B2}$ direction for the case of biaxial stress state. Symbols used here: σ_{cr}, Stress induced martensitic transformation starting stress; the blue rectangle represent the initial cell of the ensemble, the red rectangle represent the final cell of the ensemble; The yellow points represent Ti atom, and the dark points represent the Ni atoms; the tails of the atoms represent the trajectories of atoms.

A thermodynamic method to analyze the effect of stress on MT temperature is the use of the Clausius-Clapyeyron relationship, which can be expressed as follows for a uniaxial stress:[31]

$$\frac{d\sigma}{dT} = -\frac{\Delta H_V}{T_0 \Delta \varepsilon}, \tag{4}$$

where ΔH_V is the enthalpy change of the transformation per unit volume, σ a uniaxial stress, $\Delta\varepsilon$ a transformation strain, and T_0 the temperature where $\Delta G^{P\to M}=0$ ($\Delta G^{P\to M}$ is the chemical free energy change per mole).

It should be noted that Eq. (4) is only valid for uniaxial tension. For the case of biaxial stress state in the present study, the relationship between the stress in tensile direction and temperature can be easily derived as the following by a standard thermodynamic approach

$$\frac{d\sigma}{dT} = -\frac{\Delta H_V}{T_0(\Delta \varepsilon_{11} - \Delta \varepsilon_{33})}, \tag{5}$$

where $\Delta\varepsilon_{11}$ and $\Delta\varepsilon_{33}$ are the transformation strains in the tensile and compressive direction respectively, σ the stress in tensile direction.

For the MD simulations in the present study, $M_s=196$ K, $A_f=254$ K. Following the conventional assumption that $T_0=\frac{1}{2}(M_s+A_f)$, which is widely used in martensite literature,[32] T_0 is calculated to be 225 K. At a given temperature, by calculating the variation of the Parrinello-Rahman cell axis lengths during stress-induced MT in three dimensions (for example, 260 K), the transformation strain in three dimensions $(\Delta\varepsilon_{11},\Delta\varepsilon_{22},\Delta\varepsilon_{33})$ can be obtained, then the value of $\Delta\varepsilon_{11}-\Delta\varepsilon_{33}$ can be obtained at the given temperature. Considering the transformation strains are weakly temperature dependent and do not change greatly with temperature, the value of $\Delta\varepsilon_{11}-\Delta\varepsilon_{33}$ are averaged at different temperature. In the present study, the averaged $\Delta\varepsilon_{11}-\Delta\varepsilon_{33}$ from $B2$ to $L1_0''$ under biaxial stress state is 8.256%.

The enthalpy change of phase transformation can be calculated with $\Delta H=\Delta U+P\Delta V$, where P is the external pressure, which is 1.013×10^5 Pa for the present MD simulations. ΔU and ΔV are the changes of internal energy and volume per mole during the phase transformation respectively, which are 399.36 J/mol and 64 mm^3/mol, respectively in the present ensemble. Furthermore, the molar weight of our model crystal is 53.3 g/mol, and its equivalent density is 6.7 g/cm^3. Based on the above data, ΔH_V of $B2$ to $L1_0''$ phase transformation of our model crystal is obtained as -50.2 J/cm^3.

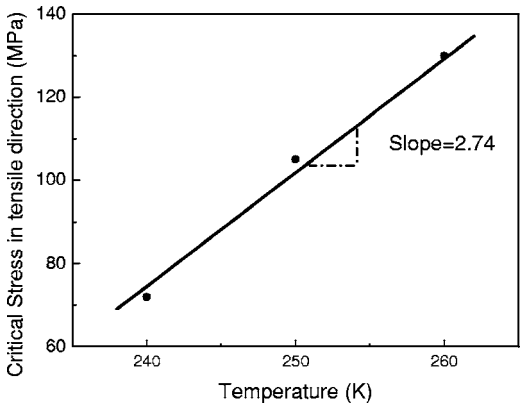

FIG. 7. Relationship between the critical stress in tensile direction for the present biaxial stress state and temperature by MD simulations. The corresponding slope predicted by the Clausius-Clapeyron equation is 2.70.

By substituting the above values into Eq. (6), the predicted slope of σ versus T curve is 2.70 MPa/K. As shown in Fig. 7, the slope of $\sigma \sim T$ curve predicted by our MD simulations is 2.74 MPa/K, which fits well with the Clausius-Clapeyron relationship. This indicates that our MD results are reliable, and the critical stress for stress-induced MT does increase linearly with temperature, obeying the Clausius-Clapeyron equation.

B. Proving elastic softening prior to stress-induced MT by an analytical theory

Now we show that, with an analytical method, we can also prove the existence of elastic softening prior to stress-induced MT, supporting our simulation results.

In a stressed crystal, the thermodynamic potential Φ is related to the Helmholz free energy F, the stress σ_{ik}, and strains ε_{ik} as follows:[33]

$$\Phi = F - \sum_{i,k} \sigma_{ik}\varepsilon_{ik}. \tag{6}$$

The Helmholz free energy (F) of a cubic crystal in terms of the symmetry adapted strain components is given in Ref. 34. By considering only symmetry breaking terms, the Helmholz free energy (F) in our case[2,5] is

$$F = F_0 + \frac{1}{2}C'(\eta_1^2 + \eta_2^2) - \frac{1}{3}C_3\eta_1(\eta_1^2 - 3\eta_2^2) + \frac{1}{4}C_4(\eta_1^2 + \eta_2^2)^2, \tag{7}$$

where $C_3 = \frac{1}{8\sqrt{3}}(3C_{112} - 2C_{123} - C_{111})$ is a combination of the third order elastic constants, and C_4 is a combination of fourth-order elastic constants; $\eta_1 = (2\varepsilon_{33} - \varepsilon_{11} - \varepsilon_{22})/\sqrt{3}$ and $\eta_2 = (\varepsilon_{11} - \varepsilon_{22})$ are the symmetry strains appropriate for cubic system, expressed in the terms of Lagrangian strain tensor components (ε_{ij}). It is noted that $\eta_2 = (\varepsilon_{11} - \varepsilon_{22})$ also represents the $(110)[1\bar{1}0]$ shear strain, i.e., the C' shear for $(110)[1\bar{1}0]$ mode. Under volume invariance condition ($\varepsilon_{11} + \varepsilon_{22} + \varepsilon_{33} = 0$), the relationship between Lagrangian strains and the order parameters can be expressed as

$$\varepsilon_{11} = -\frac{\eta_1}{2\sqrt{3}} + \frac{\eta_2}{2}, \quad \varepsilon_{22} = -\frac{\eta_1}{2\sqrt{3}} - \frac{\eta_2}{2}, \quad \varepsilon_{33} = \frac{\eta_1}{\sqrt{3}}. \tag{8}$$

For the present biaxial stress state shown in Fig. 1, the strain energy term can be expressed as

$$\sum_{i,k} \sigma_{ik}\varepsilon_{ik} = \sigma_0(\varepsilon_{11} - \varepsilon_{33}) = \sigma_0\left(-\frac{\sqrt{3}}{2}\eta_1 + \frac{\eta_2}{2}\right), \tag{9}$$

where σ_0 is the tensile stress for the biaxial stress state shown in Fig. 1.

Therefore, the thermodynamic potential Φ of the stress crystal as a function of η_1 and η_2 can be written as

$$\Phi = F_0 + \frac{1}{2}C'(\eta_1^2 + \eta_2^2) - \frac{1}{3}C_3\eta_1(\eta_1^2 - 3\eta_2^2) + \frac{1}{4}C_4(\eta_1^2 + \eta_2^2)^2 - \sigma_0\left(-\frac{\sqrt{3}}{2}\eta_1 + \frac{\eta_2}{2}\right). \tag{10}$$

The elastic constant C' for the $(110)[1\bar{1}0]$ shear mode $[C'_{110}(\sigma_0)]$ can also be defined by the second derivative of thermodynamic potential Φ with respect to $(110)[1\bar{1}0]$ shear strain $\eta_2(\sigma_0) = [\varepsilon_{11}(\sigma_0) - \varepsilon_{22}(\sigma_0)]$

$$C'_{110}(\sigma_0) = \frac{\partial^2\Phi}{\partial\eta_2^2} = C' + 2C_3\eta_1(\sigma_0) + C_4[\eta_1^2(\sigma_0) + 3\eta_2^2(\sigma_0)], \tag{11}$$

where $\eta_1(\sigma_0)$ and $\eta_2(\sigma_0)$ are the equilibrium values of the strains under the biaxial stress σ_0.

As the thermodynamic potential Eq. (7) must be invariant with respect to symmetry operations (permutation of ε_{11}, ε_{22}, and ε_{33}), Eq. (7) will keep the same form for another two sets of $\eta_1(\sigma_0)$, $\eta_2(\sigma_0)$

$$\eta'_1(\sigma_0) = [2\varepsilon_{22}(\sigma_0) - \varepsilon_{33}(\sigma_0) - \varepsilon_{11}(\sigma_0)]/\sqrt{3}, \quad \eta'_2(\sigma_0) = \varepsilon_{33}(\sigma_0) - \varepsilon_{11}(\sigma_0), \tag{12a}$$

$$\eta''_1(\sigma_0) = [2\varepsilon_{11}(\sigma_0) - \varepsilon_{22}(\sigma_0) - \varepsilon_{33}(\sigma_0)]/\sqrt{3}, \quad \eta''_2(\sigma_0) = \varepsilon_{22}(\sigma_0) - \varepsilon_{33}(\sigma_0). \tag{12b}$$

By using these two sets of $\eta_1(\sigma_0)$ and $\eta_2(\sigma_0)$ respectively, one can build up the same thermodynamic potentials as Eq. (10). The second derivatives of the potential with respect to η'_2 and η''_2 yield elastic constant C' for $(101)[\bar{1}01]$ and $(011)[0\bar{1}1]$ shear mode $[C'_{101}(\sigma_0)$ and $C'_{011}(\sigma_0)]$, respectively

$$C'_{101}(\sigma_0) = \frac{\partial^2\Phi}{\partial\eta_2'^2} = C' + 2C_3\eta'_1(\sigma_0) + C_4[\eta'^2_1(\sigma_0) + 3\eta'^2_2(\sigma_0)], \tag{13}$$

$$C'_{011}(\sigma_0) = \frac{\partial^2\Phi}{\partial\eta_2''^2} = C' + 2C_3\eta''_1(\sigma_0) + C_4[\eta''^2_1(\sigma_0) + 3\eta''^2_2(\sigma_0)]. \tag{14}$$

In the following we calculate the equilibrium values of the three sets of η_1 and η_2 as a function of external biaxial stress σ_0. Actually only one set of the η_1 and η_2 needs to be calculated and the rest two sets can be obtained by relations Eqs. (12a) and (12b) and Eq. (8). Now we calculate η_1 and η_2. Consider thermodynamic potential Eq. (10); when the stressed crystal reaches equilibrium, the following conditions must be satisfied:

$$\frac{\partial \Phi}{\partial \eta_1} = C'\eta_1 - C_3\eta_1^2 + C_3\eta_2^2 + C_4(\eta_1^3 + \eta_1\eta_2^2) + \frac{\sqrt{3}}{2}\sigma_0 = 0,$$

$$\frac{\partial \Phi}{\partial \eta_2} = C'\eta_2 + 2C_3\eta_1\eta_2 + C_4(\eta_2^3 + \eta_2\eta_1^2) - \frac{\sigma_0}{2} = 0. \quad (15)$$

Generally the equilibrium order parameters $\eta_1(\sigma_0)$ and $\eta_2(\sigma_0)$ are complex functions of external stress σ_0. Noticing strains are small in the parent state (before martensite is induced), we can make a Taylor expansion and keep the terms up to second order. Then

$$\eta_1(\sigma_0) = m_1\sigma_0 + m_2\sigma_0^2,$$

$$\eta_2(\sigma_0) = n_1\sigma_0 + n_2\sigma_0^2, \quad (16)$$

Where m_1, n_1, m_2, n_2 are constants. For a first order approximation, assuming the system is harmonic (i.e., $C_3 = C_4 = 0$), from Eq. (15) one obtains

$$m_1 = -\frac{\sqrt{3}}{2}\frac{1}{C'}, \quad n_1 = \frac{1}{2}\frac{1}{C'}. \quad (17)$$

Then Eq. (16) has only two unknown constants to be determined. Substituting Eq. (16) into Eq. (15) and neglecting terms higher than second order, we obtain

$$m_2 = \frac{1}{2}\frac{C_3}{C'^3}, \quad n_2 = \frac{\sqrt{3}}{2}\frac{C_3}{C'^3}. \quad (18)$$

Thus the equilibrium value of $\eta_1(\sigma_0)$ and $\eta_2(\sigma_0)$ as a function of external biaxial stress is as follows:

$$\eta_1(\sigma_0) = -\frac{\sqrt{3}}{2}\frac{\sigma_0}{C'} + \frac{1}{2}\frac{C_3}{C'}\frac{\sigma_0^2}{C'^2}, \quad \eta_2(\sigma_0) = \frac{1}{2}\frac{\sigma_0}{C'} + \frac{\sqrt{3}}{2}\frac{C_3}{C'}\frac{\sigma_0^2}{C'^2}. \quad (19a)$$

With $\eta_1(\sigma_0)$ and $\eta_2(\sigma_0)$ we can calculate $\eta_1'(\sigma_0)$, $\eta_2'(\sigma_0)$, and $\eta_1''(\sigma_0)$, $\eta_2''(\sigma_0)$ from Eqs. (12a) and (12b) and Eq. (8). They are

$$\eta_1'(\sigma_0) = -\frac{C_3}{C'}\frac{\sigma_0^2}{C'^2}, \quad \eta_2'(\sigma_0) = -\frac{\sigma_0}{C'}, \quad (19b)$$

$$\eta_1''(\sigma_0) = \frac{\sqrt{3}}{2}\frac{\sigma_0}{C'} + \frac{1}{2}\frac{C_3}{C'}\frac{\sigma_0^2}{C'^2}, \quad \eta_2''(\sigma_0) = \frac{1}{2}\frac{\sigma_0}{C'} - \frac{\sqrt{3}}{2}\frac{C_3}{C'}\frac{\sigma_0^2}{C'^2}. \quad (19c)$$

Substituting Eqs. (19a), (19b), and (19c) into Eqs. (11), (13), and (14), respectively, and keeping terms up to second order, we can obtain elastic constant C' for the three crystallographically equivalent shear modes, $(110)[1\bar{1}0]$, $(101)[\bar{1}01]$, and $(011)[0\bar{1}1]$, respectively

$$\tilde{C}'_{110}(\sigma_0) = C'_{110}(\sigma_0)/C' = 1 - \sqrt{3}\alpha\tilde{\sigma}_0 + \left(\alpha^2 + \frac{3}{2}\beta\right)\tilde{\sigma}_0^2, \quad (20a)$$

$$\tilde{C}'_{101}(\sigma_0) = C'_{101}(\sigma_0)/C' = 1 - (2\alpha^2 - 3\beta)\tilde{\sigma}_0^2, \quad (20b)$$

$$\tilde{C}'_{011}(\sigma_0) = C'_{011}(\sigma_0)/C' = 1 + \sqrt{3}\alpha\tilde{\sigma}_0 + \left(\alpha^2 + \frac{3}{2}\beta\right)\tilde{\sigma}_0^2, \quad (20c)$$

where $\tilde{C}'_{110}(\sigma_0)$, $\tilde{C}'_{101}(\sigma_0)$, and $\tilde{C}'_{011}(\sigma_0)$ represent respectively the normalized elastic constant $C'(\sigma_0)/C'$ of $(110)[1\bar{1}0]$, $(101)[\bar{1}01]$, and $(011)[0\bar{1}1]$ shear mode at given biaxial stress σ_0; $\alpha = C_3/C'$, $\beta = C_4/C'$; $\tilde{\sigma}_0$ is the generalized stress $\tilde{\sigma}_0 = \sigma_0/C'$. It is clear that under external stress the elastic constant C' for the three "crystallographically equivalent" shear modes is no longer the same.

According to the Landau theory, C', C_3, and C_4 are positive, thus $\alpha = C_3/C' > 0$. Furthermore, from the available experimental data on Cu-based shape memory alloys,[4,5,17,20] it is found $2\alpha^2 - 3\beta > 0$. With the information above, we can conclude from Eqs. (20a)–(20c) that under the biaxial stress σ_0 along [100]-[001] direction, the elastic constant $C'(\sigma_0)$ of $(110)[1\bar{1}0]$ and $(101)[\bar{1}01]$ shear modes softens with increasing external stress σ_0, whereas $C'(\sigma_0)$ of $(011)[0\bar{1}1]$ shear mode hardens with the increasing applied stress σ_0.

Figure 8(a) shows the variation of $\tilde{C}'(\sigma_0)$ with the external stress σ_0 for three $\{110\}\langle 1\bar{1}0\rangle$ shear modes. The α and β values ($\alpha = 5.8$ and $\beta = 10.8$) here are derived from the experimentally determined C'(7.42 GPa), C_3(43.26 Gpa), and C_4 (80 Gpa) values for $Cu_{2.72}Al_{1.122}Ni_{0.152}$ shape memory alloy.[17] It is clear that with the increase of applied stress σ_0 along [100]-[001] direction, $\tilde{C}'(\sigma_0)$ hardens for $(011)[0\bar{1}1]$ shear mode, and softens for $(110)[1\bar{1}0]$ and $(101)[\bar{1}01]$ modes. It is further noted that the stress-induced softening for $(110)[1\bar{1}0]$ shear mode or hardening for $(011)[0\bar{1}1]$ shear mode are almost linear with respect to external stress. Experimentally it has been found in Cu-based shape memory alloys, C' seems to be a linear function of external stress,[5,17,20] our calculated result in Fig. 8(a) is consistent with such an observation.

Figure 8(b) also shows the variation of $\tilde{C}'(\sigma_0)$ with the external stress σ_0 for the three $\{110\}\langle 1\bar{1}0\rangle$ shear modes, but with larger α and β ($\alpha = 29$, $\beta = 54$). We can see that the variation of $\tilde{C}'(\sigma_0)$ with the biaxial stress σ_0 becomes quite nonlinear. This situation is quite similar to the our MD results in Fig. 5(b). Therefore, the analytical expression Eqs. (20a)–(20c) provides a quantitative analysis to the stress-induced softening or hardening behavior of C' along different orientations for different systems.

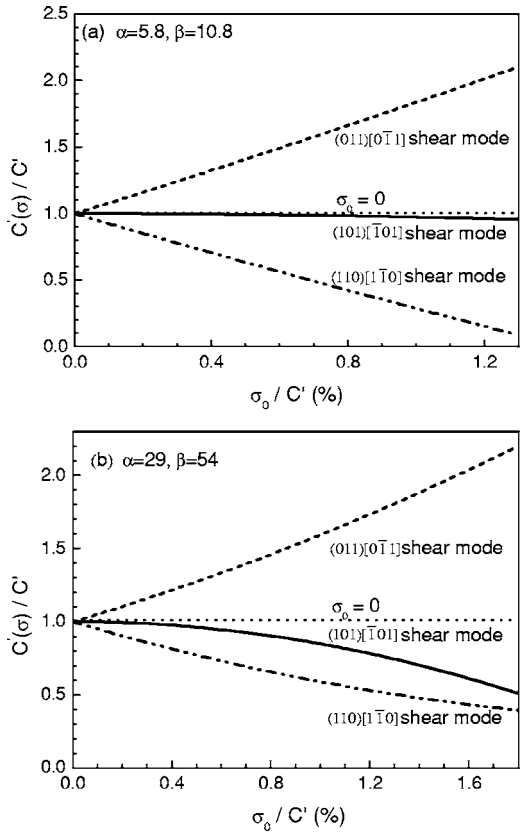

FIG. 8. Calculated normalized elastic constant $C'(\sigma)/C'$ as a function of external biaxial stress (σ_0) for three {110} ⟨110⟩ shear modes. The biaxial stress is applied alone [100]-[001] orientation as shown in Fig. 1. (a) α=5.8 and β=10.8, (b) α=29 and β=54.

It is noted that elastic softening by stress reflects the strong lattice anharmonicity of martensitic system. In this respect, our work is related to previous work[2,5,17–22] on the anharmonicity of martensitic systems. These investigations have concentrated on the measurement of high order elastic constant[2,5,17–20] and Gruneisen parameters.[2,20–22] In principle, if a complete set of second, third, and fourth rank elastic constant is known, it is possible to deduce (through Landau free energy expansion) the dependence of elastic constant C' on stress at any stress/strain level. However, a complete set of high order (in particular fourth order) elastic constant is very difficult to obtain by experiment, and the third order elastic constants are available only for a very few systems[2,5,17–22] to date. By comparison, our approach (calculating C' from the stress-strain relation) is a straightforward method and does not need any information about high order elastic constants. Therefore, the present method is a convenient and general method to calculate the softening behavior of elastic constant C' under stress; it can also provide useful information about anharmonicity of the system (i.e., higher order elastic constants).

Unlike the case of stress-induced elastic softening (which is directly linked to anharmonicity of the system), it seems that the relation between temperature-induced elastic softening and anharmonicity is not self-evident. However, it should be noted that the softening of elastic constant with temperature actually indirectly leads to an enhanced anharmonicity. This is because elastic constant is the coefficient of the harmonic terms (quadratic terms) in the Landau free energy expansion. Softening of elastic constant with temperature means that the harmonic energy decreases with lowering temperature. However, the anharmonic energies (higher order terms) are essentially insensitive to temperature changes. As the result, with lowering temperature, anharmonic energies gradually dominate the system and leads to a phase transition. Therefore, the softening of elastic constant with lowering temperature is equivalent to an enhanced anharmonicity, although the (second rank) elastic constant itself does not reflect the anharmonicity.

C. Comparison of elastic constant C' softening between temperature and stress-induced martensitic transformation

As we know, both temperature and stress can induce martensitic transformation. So it is of interest to make a comparison of elastic constant softening behavior between temperature- and stress-induced MT.

By definition, C' corresponds to the {110} ⟨1$\bar{1}$0⟩ shear modulus. Prior to temperature-induced MT, C' is naturally related to the Zener instability[35] and to the formation of basal-plane-based martensites. Considering the cubic symmetry of the crystal, the possibility of Zener instability for three crystallographically equavilent shear modes ((110)[1$\bar{1}$0], (101)[$\bar{1}$01], and (011)[0$\bar{1}$1]), are the same, i.e., the softening of C' prior to temperature-induced MT can occur in any of these three crystallographically equivalent shear modes. Furthermore, according to such a softening behavior, martensitic nuclei can be formed with any of these three crystallographically equivalent shear modes.

However, prior to stress-induced MT, the elastic constant C' softening behavior is quite different from the case of temperature-induced MT. for the present biaxial stress condition, we can see from Figs. 5(b) or Fig. 8 that C' under stress softens only in (110)[1$\bar{1}$0], (101)[$\bar{1}$01] shear modes but harden in (011)[0$\bar{1}$1] shear mode. The softening behavior of C' will cause the instability of the parent phase for the (110)[1$\bar{1}$0], (101)[$\bar{1}$01] shear modes, and thus the nucleation of the martensitic phase occurs only with (110)[1$\bar{1}$0], (101)[$\bar{1}$01] shear modes, and not with another crystallographically equivalent shear mode. This corresponds to the well-observed fact that for given stress direction only certain martensite variant(s) are induced while other variants are prohibited.

Furthermore, from the atomic movement prior to the critical stress (Fig. 6), we can see that C' softening behavior under stress is related to the microscopic strain clustering along certain orientations. For the present biaxial stress state, there exist only (110)[1$\bar{1}$0] and (101)[$\bar{1}$01] strain clusters, not (011)[0$\bar{1}$1] clusters. As discussed above, we can see that the selected formation of strain clusters is just related to the formation of a specific martensite variant under stress.

V. CONCLUSION

In the present study, by using molecular dynamic simulation, the elastic constant softening behavior prior to stress-

induced martensitic transformation has been investigated. The following conclusions are obtained.

(1) By introducing an appropriate atomic potential, we successfully simulated the superelasticity of a generic martensitic system by using molecular dynamics method.

(2) A new method for calculating the elastic constant C' under biaxial stress state is proposed, and the variation of C' prior to stress-induced martensitic transformation is simulated. It is found that the softening of elastic constant C' is a common feature both for temperature-and stress-induced martensitic transformation.

(3) The softening of C' under stress is nonlinear prior to stress induced MT, although it is approximately linear at low stress level.

(4) The softening of C' prior to stress-induced martensitic transformation is different from that prior to temperature-induced one. The softening of C' prior to stress-induced martensitic transformation occur only in some of the $\{110\}\langle 1\bar{1}0\rangle$ shear modes, depending on stress states.

(5) For the biaxial stress state, the critical stress prior to stress induced martensitic transformation also increases linearly with the increase of temperature, obeying the Clausius-Clapyeyron relationship.

(6) An analytical theory for the stress-induced precursory effects is formulated, and yields similar results as by using molecular dynamic simulations.

ACKNOWLEDGMENTS

The authors gratefully acknowledge the support of the National Science Foundation of China, a Cheungkong grant, the National Basic Research Program of China under Grant No. 2004CB619303, as well as the 111 project of China.

*Corresponding author. Electronic address:
ren.xiaobing@nims.go.jp

[1] K. Otsuka and X. Ren, Prog. Mater. Sci. **50**, 511 (2005).
[2] A. Planes and L. Manosa, Solid State Phys. **55**, 159 (2001).
[3] M. Stipcich, L. Manosa, A. Planes, M. Morin, J. Zarestky, T. Lograsso, and C. Stassis, Phys. Rev. B **70**, 054115 (2004).
[4] L. Manosa, M. Jurado, A. Planes, J. Zarestky, T. Lograsso, and C. Stassis, Phys. Rev. B **49**, 9969 (1994).
[5] A. Gonzalez-Comas, L. Manosa, and A. Planes, M. Morin, Phys. Rev. B **59**, 246 (1999).
[6] X. Ren and K. Otsuka, Scr. Mater. **38**, 1669 (2000).
[7] X. Ren, K. Taniwaki, K. Otsuka, T. Suzuki, K. Tanaki, Y. I. Chumlyakov, and T. Ueiki, Philos. Mag. A **79**, 31 (1999).
[8] X. Ren, N. Miura, K. Taniwaki, K. Otsuka, T. Suzuki, K. Tanaka, Y. I. Chumlyakov, and M. Asai, Mater. Sci. Eng., A **275**, 190 (1999).
[9] X. Ren, N. Miura, J. Zhang, K. Otsuka, K. Tanaka, T. Suzuki, Y. I. Chumlyakov, and M. Koiwa, Mater. Sci. Eng., A **312**, 196 (2001).
[10] L. Manosa, A. Gonzalez-Comas, E. Obrado, A. Planes, V. A. Chernenko, V. V. Kokorin, and E. Cesari, Phys. Rev. B **55**, 11068 (1997).
[11] S. K. Satija, S. M. Shapiro, M. B. Salamon, and C. M. Wayman, Phys. Rev. B **29**, 6031 (1984).
[12] A. Zheludev, S. M. Shapiro, P. Wochner, and L. E. Tanner, Phys. Rev. B **54**, 15045 (1996).
[13] P. Moine, J. Allain, and B. Renker, J. Phys. F: Met. Phys. **14**, 2517 (1984).
[14] M. B. Salamon, M. E. Meichle, and C. M. Wayman, Phys. Rev. B **31**, 7306 (1985).
[15] Y. Murakami and D. Shindo, Philos. Mag. Lett. **81**, 631 (2001).
[16] D. Shindo, Y. Murakami, and T. Ohba, MRS Bull. **27**, 121 (2002).
[17] A. Gonzalez-Comas and Ll. Manosa, Phys. Rev. B **54**, 6007 (1996).
[18] G. Guenin and P. F. Gobin, Metall. Trans. A **13**, 1127 (1982).
[19] B. Verlinden and L. Delaey, Metall. Trans. A **19**, 207 (1988).
[20] A. Gonzales-Comas and Ll. Manosa, Philos. Mag. A **80**, 1681 (2000).
[21] M. A. Jurado, M. Cankurtaran, Ll. Manosa, and G. A. Saunders, Phys. Rev. B **46**, 14174 (1992).
[22] A. Nagasawa and A. Yoshida, Mater. Trans., JIM **30**, 309 (1989).
[23] T. Suzuki, M. Shimono, X. Ren, and M. Wuttig, J. Alloys Compd. **355**, 183 (2003).
[24] T. Suzuki and M. Shimono, J. Phys. IV **112**, 129 (2003).
[25] T. Suzuki, M. Shimono and S. Takeno, Phys. Rev. Lett. **82**, 1474 (1999).
[26] W. C. Kerr, A. M. Hawthorne, R. J. Gooding, A. R. Bishop, and J. A. Krumhansl, Phys. Rev. B **45**, 7036 (1992).
[27] S. Kazanc, S. Ozgen, and O. Adiguzel, Physica B **334**, 375 (2003).
[28] M. Parrinello and A. Rahman, Phys. Rev. Lett. **45**, 1196 (1980); J. Appl. Phys. **52**, 7182 (1981).
[29] J. M. Sanchez, J. R. Barefoot, and J. K. Tien, Acta Metall. **32**, 1511 (1984).
[30] M. Shimono and H. Onodera, Scr. Mater. **44**, 1595 (2001); Mater. Trans., JIM **45**, 1163 (2004).
[31] *Shape Memory Materials*, edited by K. Otsuka and C. M. Wayman (Cambridge University Press, Cambrige, 1998), p. 25.
[32] C. M. Wayman and H. C. Tong, Scr. Metall. **11**, 341 (1977).
[33] E. V. Gomonaj and V. A. L'vov, Phase Transitions **A47**, 9 (1994).
[34] M. P. Brassington and G. A. Saunders, Phys. Rev. Lett. **48**, 159 (1982).
[35] C. Zener, Phys. Rev. **71**, 846 (1947).